



Does swirl number affect the radiative and convective heat transfer from diffusion hydrogen-methane blended flames?

Ben White^{a,*}, Burak Goktepe^a, Richard Marsh^a, Steve Morris^a, Andrew Price^b

^a Cardiff University, United Kingdom

^b CR Plus, United Kingdom

A B S T R A C T

Industries are exploring hydrogen fuel switching to achieve net-zero targets. Pure hydrogen combustion eliminates carbon dioxide emissions, but this could adversely affect the heating performance since much of the radiative heat transfer from hydrocarbon flames originates from hot carbon dioxide molecules and soot particles, absent from hydrogen combustion.

To investigate the effect of swirl number on a flame's heat transfer, a generic swirl burner was operated at 25 kW thermal input, with three geometric swirl numbers, a fixed equivalence ratio of 1.0 and methane-hydrogen blends of 0–100 % by volume. Hydrogen and methane exhibited different radiative and convective heat transfer properties.

Results showed that increasing geometric swirl number produced shorter flames with lower radiative heat transfer. The maximum radiative heat flux of a flame occurred between ~50–70 % along the flame's length. Increasing hydrogen blending resulted in an increased flame temperature. 25–50 % hydrogen blending enhanced methane flame's radiative heat transfer, while further blending reduced it. Local convective heat flux correlated well with local gas temperature, regardless of fuel.

The ratio of radiation to convection was greatest early in the flame, with convection increasing along the flame's length. Both heat transfer modes decreased at similar rates with radial distance from the burner centreline.

This study examined the temperature of a steel slab using a thermocouple array to analyse heat transfer. While the hypothesis was not confirmed, results showed process temperatures are influenced by multiple factors. Steel temperatures were setup specific. Heat flux, flame, and product temperature measurements provided a strong heat transfer assessment.

1. Introduction

With the growing global imperative to reduce carbon dioxide emissions, industrial sectors must take urgent and bold steps, such as net zero carbon fuel switching, to address the impacts of climate change and meet their net zero targets [1].

With the UK hydrogen strategy aiming to develop a thriving 10 GW capacity low carbon hydrogen sector by 2030 [2], research and development of fuel switching industrial applications is vitally important to de-risk manufacturing sites' transition to net zero. Currently in the UK, the areas of generation and distribution for net-zero fuel switching are advancing with support from UK Government incentivised programmes such the Hydrogen Production Business Model [3] and Project Union [4]. The UK hydrogen strategy aims to decarbonise the “hard to electrify” industrial sectors. This includes large-scale industrial heating applications, with the steel sector expected to create the greatest demand for low carbon hydrogen, alongside chemicals [2].

The South Wales Industrial Cluster (SWIC) Plan report [5] highlights

the unknown risks involved with fuel switching, within Policy Driver 22 stating, “The need for a Fuel Switching Centre of Excellence has been identified to support our industries through the technical aspects of fuel switching away from natural gas.” However, fuel switching from natural gas to hydrogen [6], with blends, will modify the radiative heat transfer in industrial furnaces. High temperature industrial processes greatly rely on radiative heat transfer, generated by combustion [7]. In industrial heating processes that exceed one thousand degrees Celsius, literature states that 90 % of the total heat transfer is attributed to radiative heat transfer [8]. For low temperature processes, convection is expected to play a much greater role in the overall heat transfer from flames [9].

In literature, it is stated that many industrial diffusion burners may be safely operated with hydrogen fuel with little to no modification [10]. It is stated by Leicher et al. [11] that natural gas and hydrogen combustion results in similar heat flux and temperature profiles. An example of this is a Computational Fluid Dynamics (CFD) study, which concluded that 66 % heating efficiency was achieved for both natural gas and hydrogen fired furnaces, suggesting that hydrogen may be used without

* Corresponding author at: GTRC Gas Turbine Research Centre (Cardiff University), Port Talbot SA13 2BZ, United Kingdom.

E-mail address: WhiteBR@cardiff.ac.uk (B. White).

<https://doi.org/10.1016/j.tsep.2025.103568>

Received 28 August 2024; Received in revised form 12 March 2025; Accepted 3 April 2025

Available online 5 April 2025

2451-9049/© 2025 The Authors. Published by Elsevier Ltd. This is an open access article under the CC BY license (<http://creativecommons.org/licenses/by/4.0/>).

an evident impact on the heating efficiency of the furnace.

In other work, the impact of hydrogen blending was explored in a semi-industrial furnace. The hydrogen blends assessed were 0 %, 10 %, and 50 % by volume in natural gas. For these blends, the heat transfer impact was considered unchanged. It is also stated that in other simulated scenarios, if the furnace was unsuitably controlled, a significantly reduced heat flux occurred [12].

In a similar study, hydrogen and natural gas blends of 0 %, 10 %, 30 %, 50 % and 100 % were used in a semi-industrial furnace. The study concluded that there are some challenges and open questions regarding the radiative characteristics of hydrogen and natural gas flames. The study suggested that there is a high level of specialization and optimization required in thermal processing industries. The use of hydrogen admixtures in process heating will therefore require an equivalent level of specialization and optimization to avoid compromising the process' performance [13].

Similarly, the testing of 0 % to 50 % natural gas and hydrogen blends at 100 kW, 200 kW and 300 kW furnace conditions has been performed in literature. Based on the exhaust gas temperature and thermal load on the experimental cooling tubes, a similar heat transfer was assumed across the hydrogen blending cases [14]. However, the distinctions between radiative and convective heat transfer are not made and the 50 % limit on hydrogen blending cannot display the full impact of pure hydrogen combustion on a process.

Mayrhofer et al. [15] describe an experiment conducted using hydrogen-natural gas blends ranging from 0 % to 40 % in a semi-industrial scale furnace with a capacity of 165 kW. The furnace operated with a 470 °C air preheat and utilized a radiant tube for indirect steel heating. By analysing the energy balance through flue gas losses, the study found that blending natural gas with 40 % hydrogen improved the furnace efficiency from 70.67 % to 71.84 %. While the efficiency change is marginal and the blending limited to 40 % in this experiment, the results demonstrate the potential use of radiant tubes as an alternative approach for heating applications with hydrogen blending.

Xu et al. [16] investigated the impact of increasing hydrogen concentration on the heat transfer to a lab scale furnace wall. Their findings indicated a marginal increase in overall heat transfer from the gas to the wall, with the furnace gas' radiative heat transfer contributing between 68.8 % and 82.3 % of the total heat flux. In this study by Xu et al. [16], fuel switching from natural gas to hydrogen resulted in a 29.4 % enhancement in radiative heat transfer from the gas to the wall, accompanied by a 16.8 % reduction in convective heat transfer. This led to an increase of 15 % in total heat transfer efficiency.

Daurer et al. [17] conducted an experimental study, supported by 3D CFD analysis, using a semi-industrial furnace with a burner delivering up to 120 kW of power. The research measured heat transfer efficiency to various cooling lances under hydrogen-enriched natural gas, with hydrogen levels ranging from 0 % to 100 %. Experimentally, it was observed that increasing hydrogen content led to an increase in the heat flux from the flame to the cooling lances. The CFD simulations identified the radiative and convective heat transfer components for each cooling lance. For many of the cooling lances, the CFD simulations did not show significant changes with varying hydrogen blends. Despite this, the study concluded that hydrogen enrichment could improve this process' efficiency by 5–10 %, driven by higher temperatures and enhanced heat transfer within the furnace.

This work therefore will seek to provide insights into the individual radiative and convective heat transfer modes of 0–100 % hydrogen-methane blended flames, that may be applied to a broad range of processes, since there is a large degree of specialisation amongst specific industrial heating processes. It is then valuable to evaluate the findings of this study to the existing literature data, which predominantly addresses hydrogen and natural gas blends of 0 % to 50 % by volume, at the semi-industrial scale.

The relationship between process temperature and the relative contribution of independent heat transfer modes is as expected, given

the fundamental relationship of radiation and convection with temperature. As temperature increases, convection is expected to linearly increase, whereas radiation is expected to increase relative to T^4 . The fundamental equations for radiative and convective heat transfer are shown as Equations (1) and (2) respectively, where ϵ is emissivity, σ is Stephan-Boltzmann constant, A is the area of heat transfer, T is temperature and h in convective heat transfer coefficient [8]:

$$Q_{\text{rad}} = \epsilon \sigma A T^4 \quad (1)$$

$$Q_{\text{conv}} = hA(\Delta T) \quad (2)$$

Convective heat transfer is the result of conductive heat transfer, through a fluid flow to the surface. This is driven by a temperature difference, located at a boundary layer, close to the heat transfer surface. The thickness and development of this boundary layer is dependent upon the properties of the flow and of the fluid [8]. In the literature, direct flame impingement has been found to significantly increase the convective heat transfer from a flame to a product. Whilst not all processes adopt this set up, it can provide an opportunity to increase productivity or decrease fuel consumption [9].

Radiative fraction, χ_R , is a parameter used to characterise the radiative heat transfer from flames, Q_{rad} , relative to the flame's total heat release, due to the chemical reaction $m_{\text{fuel}}\Delta H_c$, where m_{fuel} is the fuel mass flowrate and ΔH_c is the heat of combustion [18]. This relationship is given by Equation (3):

$$\chi_R = Q_{\text{rad}}/m_{\text{fuel}}\Delta H_c \quad (3)$$

In the literature, radiative fraction has been shown to increase with global residence time, τ_G [19]. Previous research in this area has studied the effect of residence time on the radiative fraction of pure hydrogen and pure methane flames [19]. According to the findings, for the same residence time, pure hydrogen flames exhibit a lower radiative fraction than pure methane flames. The reduced radiative heat flux from hydrogen flames is typically due to the absence of soot particles and carbon dioxide molecules, with soot particles in particular acting as black body emitters [20]. Global residence time is defined by Equation (4), where the flame length is L_f and the jet velocity of the fuel is U_f [21].

$$\tau_G = L_f/U_f \quad (4)$$

When adjusting the hydrogen-methane blend at a constant thermal input power, the fuel jet velocity (U_f) varies with the changing densities of the fuel blends. Global residence time can also be modified by altering the swirl number of the burner [22]. Swirling flames are common in industrial heating processes [23]. Increasing the geometric swirl number, S_g , is expected to decrease flame length, L_f , thereby decreasing the global residence time [22]. For a diffusion flame, the central fuel jet velocity, U_f , should remain unchanged in this case.

It is of research value to analyze the impact of swirl number and hydrogen blending on radiative fraction [18]. Cardiff University's Gas Turbine Research Centre (GTRC) has previously used the Generic Swirl Burner (GSB) with hydrogen-methane blends to assess the effect of swirl number on combustion emissions, particularly NOx [24]. In this work, the same geometric swirlers have been used to investigate the influence of S_g on the radiative heat transfer of hydrogen-methane blends.

The work on flame radiation by Schefer et al [19] describes how radiative power from turbulent jet flames can be represented in terms of non-dimensional radiant power, C^* , in Equation (5):

$$C^*(z/L) = \frac{4\pi R^2 q_{\text{rad}}(z/L)}{Q_{\text{rad}}} \quad (5)$$

In this case, R is the radial distance from the flame centreline, $q_{\text{rad}}(z/L)$ is the radiative heat flux profile along the flame length L_f , and Q_{rad} is the total radiative heat from the flame. This work is of interest, as it is stated that for both hydrocarbon and hydrogen jet flames, the

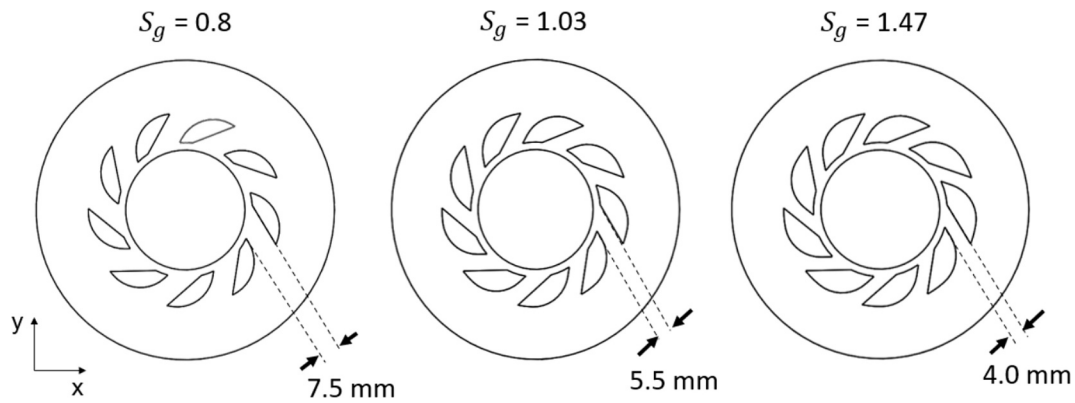


Fig. 3. The GSB swirlers, $S_g = 0.8, 1.03, 1.47$, with characteristic measurements.

expected to vary in industrial conditions with lower confinement ratios.

The first element of this research aimed to quantify differences in the radiative heating of hydrogen-methane blended flames, evaluating the effect of geometric swirl number. The radiative heat flux was measured using a Huskeflux GG01 Gardon gauge. Employing a thermocouple hot-cold junction principle, the Gardon gauge facilitated real-time monitoring of heat flux, generating a potential difference proportional to incoming irradiance [31]. To isolate the signal produced by radiative heat transfer only, a sapphire lens was placed over the Gardon gauge's black-coated thermopile sensor, eliminating the convective heat transfer components [32].

The Gardon Gauge manufacturer's data specifies a $\pm 2.0\%$ non-linearity margin of error, calibrated at 100 kW/m^2 . This corresponds to an absolute error of $\pm 2.0 \text{ kW/m}^2$ for all heat flux measurements. Consequently, error bars of $\pm 2.0 \text{ kW/m}^2$ were included in all figures presenting heat flux measurements obtained using the Gardon Gauge [32].

When accounting for transmissibility losses involved with using a sapphire lens, the average transmittance of sapphire was factored in during the calculation of radiative heat flux. For the transmissibility of Sapphire, a range of 84–86% is quoted in literature, comparable to glass

[32,33,34]. According to the manufacturer's data specification, the Gardon Gauge had a viewing angle of 150° [32], when using the sapphire lens.

Equation (3) was used to find the radiative fraction of a flame, dividing the radiative heat transfer, Q_{rad} , by the 25 kW thermal input power. To find Q_{rad} , the "line of sight radiative heat flux profile" was integrated over its emitted area, at the radial distance of 100 mm.

The second element of this work was to compare the radiative and convective heat transfer modes from hydrogen and methane flames, for a fixed S_g of 1.47. To calculate the convective heat flux component, it was assumed that only radiative and convective heat flux modes contributed to the total heat flux. Convective heat flux may then be calculated as the difference between measured total heat flux and the measured radiative heat flux. Total heat flux was measured using the same Gardon Gauge, but without the sapphire lens on the sensor's surface. The respective values of radiative and convective heat transfer were expected to vary in intensity along the length of the flame [25], in addition to the radial direction from the flame, so measurements were taken from a variety of axial and radial locations.

For hydrogen-methane blends, assessing the effect of S_g and blending on radiative heat transfer, all measurements were taken from 100 mm

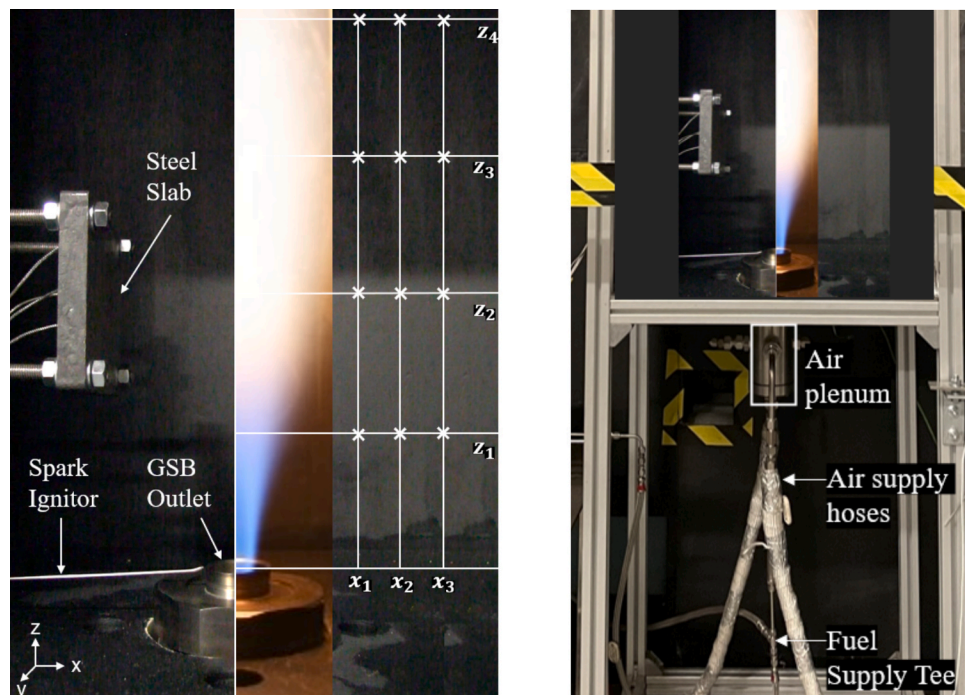


Fig. 4. Experimental set up, with thermocouple monitored steel slab, igniter, GSB nozzle. (Axis not to scale, for demonstration purposes only).

radially from the Z-axis centreline, along the height of the flame ($z_1 = 120$ mm, $z_2 = 240$ mm, $z_3 = 360$ mm, $z_4 = 480$ mm). This coordinate system is shown in Fig. 4. When comparing the convective and radiative heat transfer modes of hydrogen and methane flames, measurements were taken at further radial locations, in the X-axis direction from the flame ($x_1 = 100$ mm, $x_2 = 125$ mm, $x_3 = 150$ mm). For each radial location assessed, measurements were made along the length of the flame, as done previously, shown in Fig. 4.

K-type thermocouple temperature measurements were taken at the burner Z-axis centreline, for each experimental case at each height. As seen in Fig. 4, a mild steel slab (140 mm × 140 mm × 20 mm) was positioned adjacent to the flame, 100 mm offset from the burner Z-axis centreline. The centre point of the steel slab was aligned to z_2 , a height 240 mm along the Z-axis from the burner nozzle exit. This positioned the steel slab to be at a height, estimated to be within the band of maximum radiative heat flux, at $0.5\text{--}0.7 L_f$, for each experimental case [19]. The distance of the steel slab to the burner Z-axis centreline was the same as the radiative Gardon Gauge measurements, at a radial distance of 100 mm, for comparability. The position of the steel slab remained unchanged to effectively demonstrate any alterations in heating performance during fuel switching. Although the steel slab would not behave as a black body, the emissivity of a machined face of the mild steel slab was estimated to be $0.2\text{--}0.3$ [35]. An exact value could not be accurately determined without a calibrated emissometer. Yet, the steel slab's temperature response will remain as a semi-quantitative approach to evaluating the changes in heat transfer between hydrogen-methane blended flames to an industrially relevant product. It was hypothesised that the measured radiative heat flux will correlate to the steady state temperature of the steel slab.

The temperature profile of this steel slab was monitored continuously by four K-type, surface mounted thermocouples. Three thermocouples were aligned vertically, at 35 mm intervals along the steel slab's centreline. This centreline was parallel to the burner centreline, along the Z-axis. An additional thermocouple was positioned at an offset of 35 mm in the Y-direction, as shown in Fig. 5.

The locations of the surface thermocouples on the steel slab aimed to allow investigation into the location of maximum heat transfer, manifesting as the temperature profile of the plate. The arrangement of thermocouples examined if the point of maximum heat transfer had an impact on the temperature profile of the steel slab, or if conductive heat transfer through the steel compensated for this. Where the thermocouple measurements were comparatively even, conduction was assumed to be

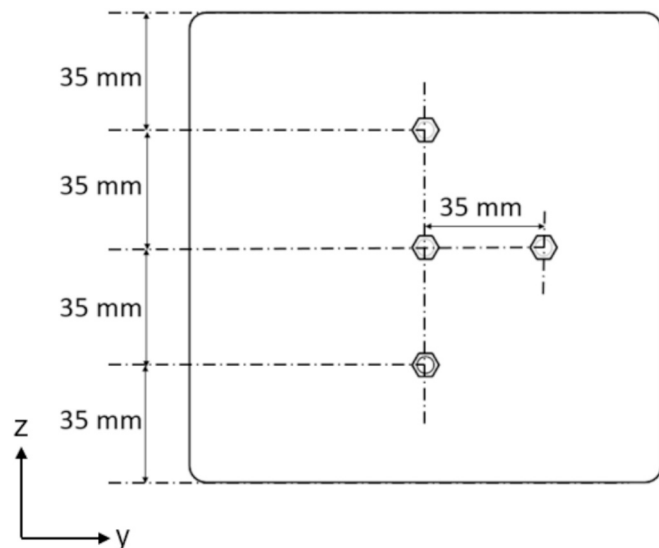


Fig. 5. Mild steel slab, showing the location of the measurement thermocouples.

dominant and an average temperature, T_{avg} , was taken across the plate.

To assess the practical heating performance of hydrogen-methane blends, the temperature of the steel slab was measured over time. The steel slab increased in temperature with time due to the heat transfer from the flame. Natural convection and radiative heat losses from the steel slab increased as a function of the temperature of the steel slab [8]. The rate of temperature increase asymptotically approaches zero where the radiative and convective losses from the steel slab approach the heat transfer from the flame to the steel slab [36]. Flames of higher heat flux to the steel slab achieved higher steel slab temperatures as a result.

Each test on the steel slab was performed for a maximum of 60 min, balancing time restraints and fuel demands with confidence that the steel slab temperature had reached a steady state. Each test started with the steel slab at 20°C . For safety reasons, the ignition for each test point was performed with methane, before adjusting the fuel composition to the desired condition, which took approximately 5 min. Data was only taken from the point at which the intended fuel composition was attained. Hence, temperature plots begin at 35°C , the earliest common point at which all tests had successfully attained the correct fuel compositions.

Thermocouples develop inaccuracies due to radiative heat losses from the thermocouple itself, reading lower temperatures than the gas temperature that it is situated in, hence the thermocouple values for flame and gas temperatures were corrected. The thermocouple was considered to be convectively heated by the local gas, rising in temperature and emitting radiative heat as a result. By equating the convective heat transfer between the gas and the thermocouple to the radiative heat between the thermocouple and the surroundings, the true gas temperature was found. Empirical Nusselt number correlations were used to find the convective heat transfer components of the equation, considering the thermocouple as a cylinder in crossflow, a widely used methodology [37]. For the thermocouple data produced, instrumentation uncertainty may be considered as the greater of $\pm 2.2\text{--}2.5$ degrees Celsius or $\pm 0.75\%$ as per the thermocouple supplier [38,39]. For lower, ambient temperatures, a ± 2.5 degrees Celsius uncertainty should be used. For greater flame temperatures, a $\pm 0.75\%$ uncertainty should be used.

Table 1 contains the flame lengths in each experimental case. These flame lengths were calculated by digitally averaging a 10 s video (25 frames per second) of each flame. A DSLR camera was used for direct flame photography. The averaged images were digitally binarised with a threshold limit of 30 %, to define the visible flame. The 30 % threshold value was chosen due to its ability to produce a precise contour of the flame tip using the binarised image, which aligned with the flame tip in the averaged images with acceptable sensitivity. The axial distance, on the Z-axis, from the burner nozzle exit to the furthest visible flame tip was used to define flame length, L_f . The averaged images can be seen in Fig. 6. The residence times for each experimental condition are also included in Table 1, using the same methodology shown in Equation (4). For this, the flame's length, L_f , and the fuel jet velocity, U_{jet} are used.

Table 1 also presents the relevant fuel and air flow rates, with adiabatic flame temperatures (AFT) included, calculated using the ANSYS Chemkin Equilibrium model. AFT is the temperature achieved by a flame if all the heat of combustion is transferred to the combustion products, with no heat loss to the surroundings [40].

A constant 25 kW fuel supply was delivered to the GSB through the central fuel lance, based on the fuel blend's lower heating value (LHV). The fuel supply was kept constant so that radiative heat flux measurements could be directly comparable, relative to a constant input power. The hydrogen and methane fuel inputs were controlled by a series of mass flow controllers and measured with Coriolis flow meters to record the mass flowrates of fuel and air. A stoichiometric mixture of fuel and air was used, maintaining an equivalence ratio of 1.0 across all test points.

Table 1 presents the jet velocities of the fuel blends, that were calculated by Equation (10), where D is the fuel orifice diameter (5 mm),

Table 1
Experimental conditions matrix.

S_g	Hydrogen % (v/v)	\dot{m}_{CH_4} (g/s)	\dot{m}_{H_2} (g/s)	\dot{m}_{air} (g/s)	LHV (MJ/kg)	L_f (m)	U_{jet} (m/s)	Residence time (ms)	AFT (K)
0.8	0	0.500	0.000	8.595	50.000	0.486	35.583	13.67	2229
	25	0.454	0.019	8.463	52.815	0.508	43.109	11.78	2242
	50	0.384	0.048	8.259	57.816	0.498	54.673	9.11	2262
	75	0.262	0.099	7.907	69.168	0.478	74.715	6.34	2298
	100	0.000	0.208	7.146	120.000	0.473	117.952	4.01	2343
1.03	0	0.500	0.000	8.595	50.000	0.452	35.583	12.70	2229
	25	0.454	0.019	8.463	52.815	0.465	43.109	10.79	2242
	50	0.384	0.048	8.259	57.816	0.477	54.673	8.72	2262
	75	0.262	0.099	7.907	69.168	0.433	74.715	5.79	2298
	100	0.000	0.208	7.146	120.000	0.398	117.952	3.37	2343
1.47	0	0.500	0.000	8.595	50.000	0.436	35.583	12.25	2229
	25	0.454	0.019	8.463	52.815	0.456	43.109	10.58	2242
	50	0.384	0.048	8.259	57.816	0.441	54.673	8.07	2262
	75	0.262	0.099	7.907	69.168	0.385	74.715	5.16	2298
	100	0.000	0.208	7.146	120.000	0.341	117.952	2.89	2343

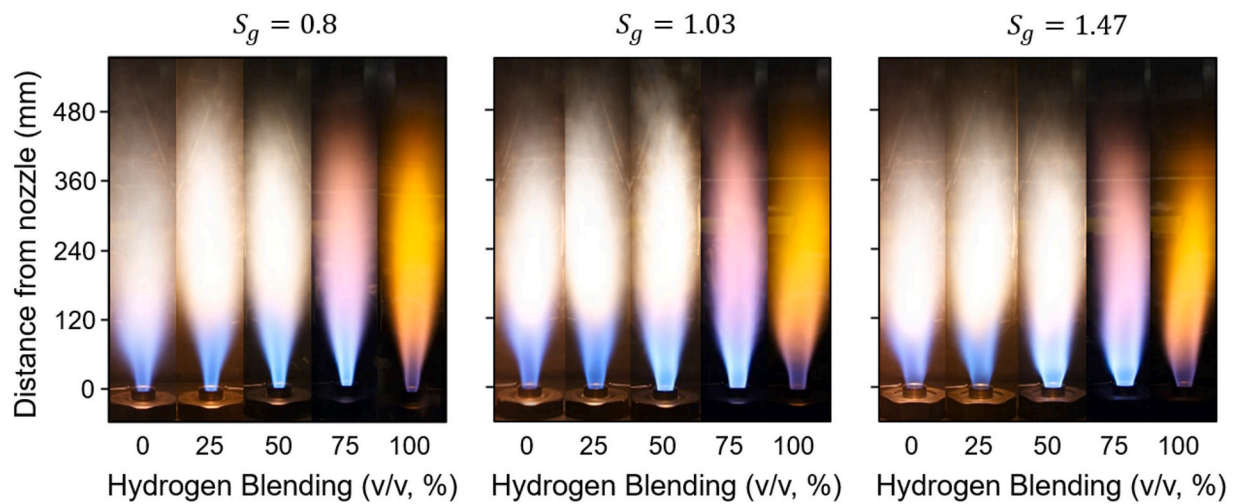


Fig. 6. Average diffusion flame images of hydrogen-methane blends at stoichiometric conditions, for three geometric swirl numbers, at ambient conditions.

ρ is the density of the fuel, Q is the fuel input power (25 kW) and LHV_{blend} is the lower heating value of the blend on a mass basis:

$$U_{jet} = \frac{Q}{\rho \cdot \pi \cdot (0.5 \cdot D)^2 \cdot LHV_{blend}} \quad (10)$$

The radiative and total heat flux data from the Gardon Gauge, in addition to the thermocouple measurements were collected with a National Instrument compact DAQ, monitored and recorded by its Flex-Logger software. The sampling rate for measurements was 1 Hz.

3. Results and discussion

Fig. 6 contains the averaged flame images in each experimental case, visually displaying how hydrogen blending, and geometric swirl number, affect the visible flame length and appearance of swirling hydrogen-methane blended diffusion flames. As S_g increases, flame length decreases for the same fuel composition, as indicated in **Table 1**.

Fig. 7 shows how the measured visible flame lengths and calculated residence times vary with hydrogen-methane blending and geometric swirl number, where increasing S_g shortens the length of the flame, for the same fuel composition. Residence times were calculated using Equation (4), considering the fuel jet velocity and flame length. Increasing hydrogen blending resulted in an increase in fuel jet velocity at a constant thermal input, due to the low density properties of gaseous hydrogen. This same increase in fuel jet velocity saw a decrease in the residence time, as suggested by the relationship in Equation (4). Increasing hydrogen blend also increased the reactivity of the fuel

mixture. Increasing S_g was expected to decrease the visible flame length for the same fuel blend, which was observed. Hence, increasing S_g decreased the calculated global residence time of the fuel, in this diffusion flame set up. The longest flame lengths for the $S_g = 0.8$, $S_g = 1.03$ and $S_g = 1.47$ were at 25 % hydrogen blending, 50 % hydrogen blending and 25 % hydrogen blending, respectively. In these experiments, hydrogen-methane blending impacted the global residence time, τ_G , more than geometric swirl number, S_g .

The visual flame length measurements displayed in **Fig. 7** may be used to more quantifiably visualise the effect of fuel blend and S_g on the axial flame length, captured visually in **Fig. 6**. Equation (4) was then used to calculate global residence time, as per the methodology used in the literature by Turns and Myhr [21].

Fig. 8 displays the flame temperature measurements along the Z-axis centreline of the burner, relative to the flame's length, L_f , for each experimental case. In each instance, temperatures were greatest, earlier in the flame, between $z/L_f = 0.3-0.7$. Since higher S_g led to shorter flame lengths, temperature measurements were taken farther along the flame's nominal length relative to its total length, z/L_f .

The general trend suggests that by increasing hydrogen blending, greater flame temperatures are achieved, which was expected when considering the corresponding adiabatic flame temperatures presented in **Table 1**.

Fig. 9 shows the radiative fraction of hydrogen-methane blends and the effect of S_g . It can be seen that increasing S_g results in a decrease in the radiative fraction for a given fuel composition. It is suggested that this decrease in radiative fraction is due to the reduced global residence

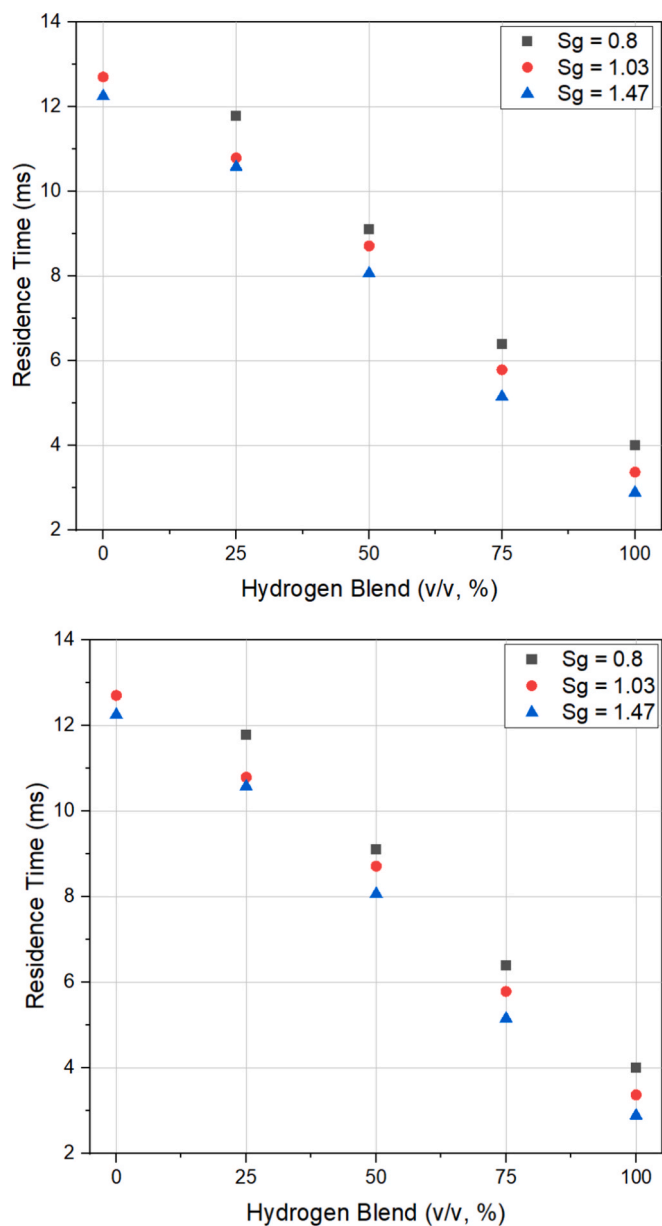


Fig. 7. Measured visible flame lengths and calculated residence times with respect to hydrogen blending and geometric swirl number.

time caused by higher S_g . For the $S_g = 0.8$ case, radiative fraction decreased with hydrogen blend. However, without a 0% hydrogen case, a true trend may not be explicitly described. As mentioned, this data point was not achieved due to the lifting and eventual unstable blowoff of the $S_g = 0.8$, methane flame. The maximum radiative fraction for the $S_g = 1.03$ case was measured with the 25% hydrogen blend. For the $S_g = 1.47$ case, the maximum radiative fraction was measured with the 50% hydrogen blend. Both the $S_g = 1.03$ and $S_g = 1.47$ cases displayed an inverse parabolic relationship between hydrogen blend and radiative fraction. This relationship is expected to represent a trade-off between elevated flame temperatures from increased hydrogen blending, and the decrease in highly radiating species, such as soot particles and carbon dioxide molecules due to the same increase in hydrogen blending. In this experimental set up, moderate hydrogen blending of 25–50% generally enhanced the radiative fraction of the flame, whereas higher hydrogen blending cases saw a decrease in radiative fraction, when compared to a pure methane base case. These results in Fig. 9 confirm the challenges and open questions regarding the radiative properties of hydrogen and

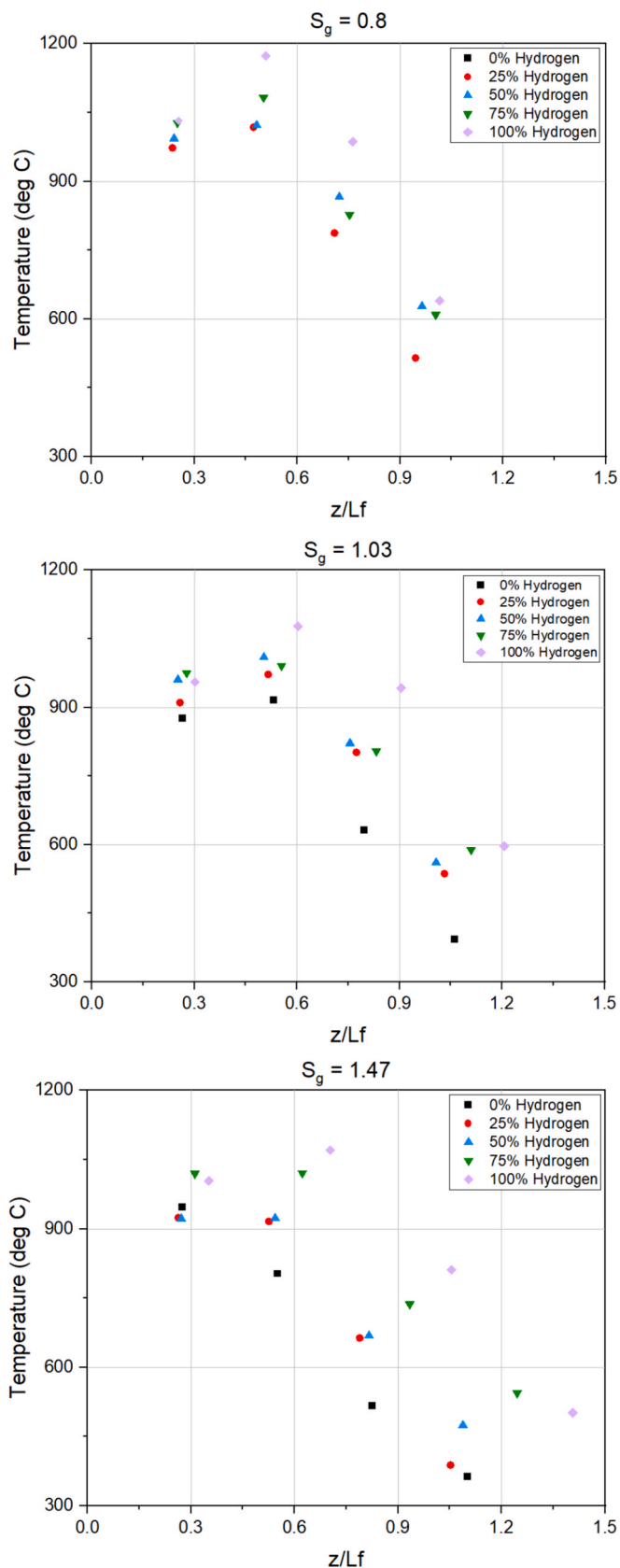


Fig. 8. Measured temperature along the nominal length of the flames with respect to hydrogen blending and geometric swirl number.

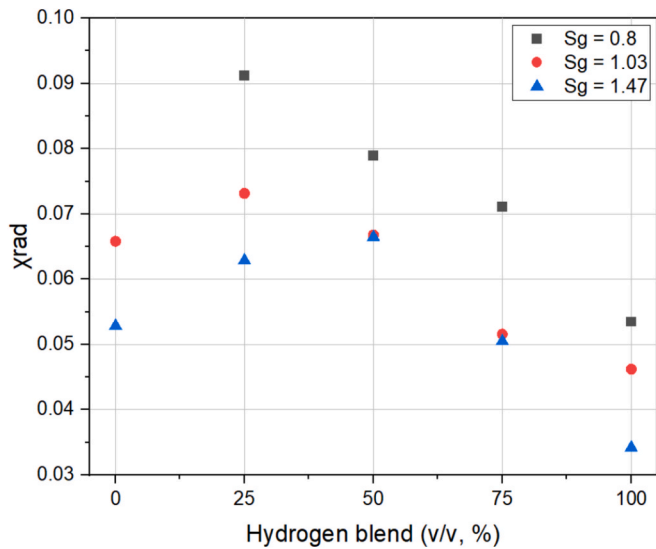


Fig. 9. Radiative fraction, χ_{Rad} , with respect to hydrogen blending and geometric swirl number.

methane flames by Leicher et al [13].

The observed increase in radiative fraction at 25–50 % hydrogen blends may explain how Mayrhofer et al. [15] and Meynet et al. [14] reported no negative impact on heating efficiency with hydrogen blends up to 40 % and 50 % respectively. Yet, as shown in Fig. 9, beyond 50 % hydrogen blending by volume, radiative fraction decreased. This study does not directly contradict this existing literature. Whilst Fig. 9 displays the radiative properties of the flame, Mayrhofer et al. [15] and Meynet et al. [14] focused on a whole-system approach, considering both radiative and convective heat transfer modes, but only considered blends up to 50 %. This work extends the analysis to hydrogen blends of up to 100 %, albeit on a laboratory scale. It is suggested that further work be done, assessing the impact on semi-industrial scale systems with blends up to 100 % hydrogen.

From the radiative fraction trends in Fig. 9, it can be stated that industrial heating processes should potentially explore a reduction in their burner’s geometric swirl number, should they wish to achieve maximum radiative heat transfer from the flame where hydrogen is blended with natural gas. Reducing the geometric swirl number of a burner maximises the flame length for a constant fuel condition. Radiative fraction shows correlation to measured flame lengths and calculated global residence time. This topic should be explored in greater depth in future studies, in particular through CFD simulation of flame residence times. A limitation of the current study lies in the absence of a validated CFD study. As this research prioritised experimental methods, the conclusions drawn are based solely on experimental results. A validated CFD study would offer the potential to better predict global residence times more accurately, further supporting the conclusions derived from the residence time calculations in Equation (4). The CFD study would also allow for particle tracking in the swirling flow to better measure the effect of swirl number on particle residence times. For this purpose, the characteristic dimensions of the GSB have been provided in Figs. 2 and 3.

Fig. 10 shows the distribution of radiative heat flux along the nominal axial position along the flame, z/L_f . The trend in Fig. 10 indicates that there is a location of maximum radiative heat flux between ~ 50–70 % of the visible flame length, $or_z/L_f = 0.5–0.7$. Flames with shorter lengths have their maximum radiative heat flux location closer to the burner nozzle, while longer flames have this location shifted downstream. This agrees with the work performed by Sivanthanu and Gore [25], on methane, ethane and ethene flames whereby the distribution of radiative heat flux, relative to distance along the flame’s length. This infers that this relationship may also be applied to

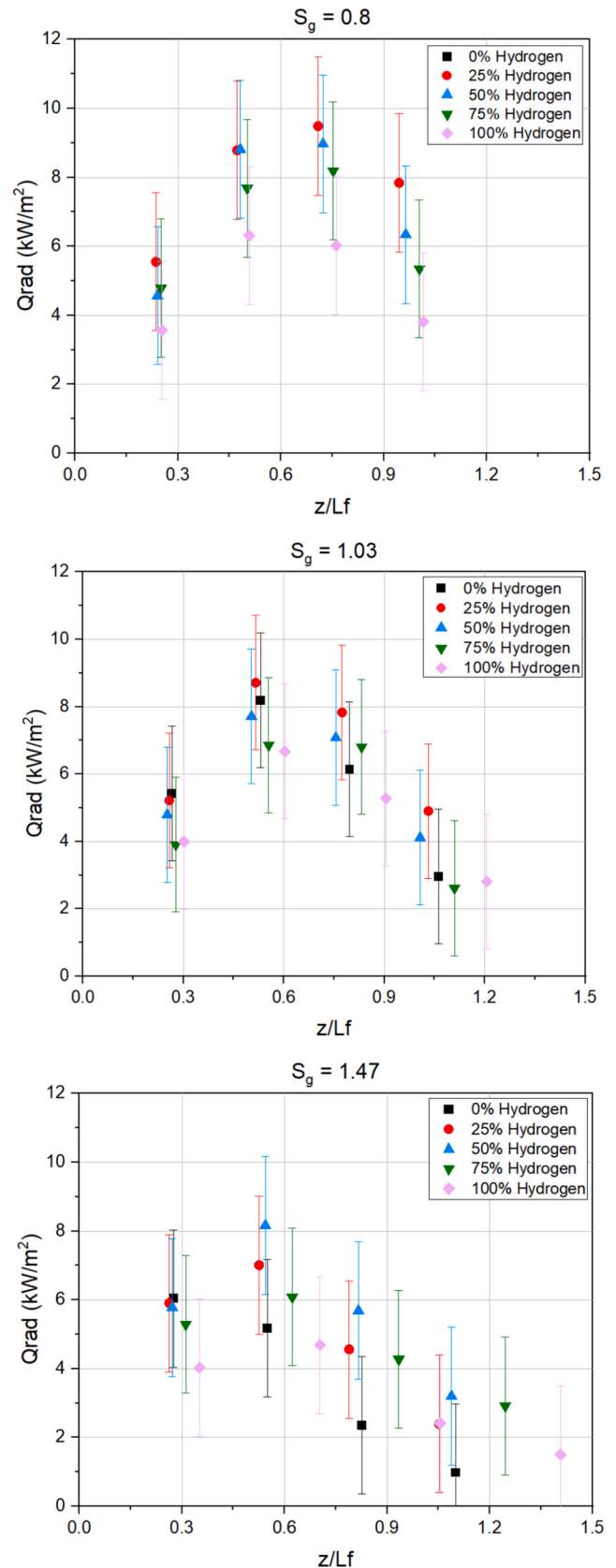


Fig. 10. Measured radiative heat flux along the nominal length of flames with respect to hydrogen blending and geometric swirl number.

hydrogen-methane blends. To determine the location along the flame of maximum radiative heat flux with greater precision it is advisable to use reduced measurement intervals along the flame's length.

Despite the significant error bars in Fig. 10, the overall trend in radiative heat flux remains consistent across all experimental cases, even with the most conservative interpretation of the error. This indicates that the relationship between nominal flame length and radiative heat flux is unaffected by the error bars, confirming the validity of the observed trend.

Fig. 11 displays the dimensionless radiative power, C^* , as a function of the nominal axial position (z/L_f) along the flame length to better evaluate how S_g and hydrogen blending affect the nominal location of maximum radiative heat flux along a flame's length. Previous studies by Schefer et al [19] and Sivathanu et al [25], have demonstrated that for turbulent jet flames, this data typically collapses onto a single curve, independent of the fuel used. In this analysis, for the lowest swirl case tested, $S_g = 0.8$, the relationship between C^* and z/L_f does indeed closely align with the trend reported by Schefer et al. [18] for turbulent jet flames. As S_g is increased, the observed data progressively deviates from the expected trend, indicating that this universal relationship for jet flames does not hold true for higher swirl cases. In most cases, the maximum value of C^* occurred between $z/L_f = 0.5$ – 0.7 . This range aligns with the findings of Sivathanu et al. [25] despite deviating from the precise curve suggested by that literature, when testing higher swirl numbers.

Fig. 12 shows the transient response of the steel slab temperature, starting from 35 °C, approaching steady state within an hour. The temperature profile of the steel slab was evenly distributed, with all thermocouples producing very similar values throughout the length of the test. This suggests that the conductive heat transfer through the steel slab offset any differences in local heat flux distribution to the steel slab.

Fig. 13 displays the temperatures of the steel slab, once it had achieved steady state. The $S_g = 1.03$ swirl burner produced lower temperatures with increased hydrogen blending. The $S_g = 0.8$ and $S_g = 1.47$ cases displayed unique relationships between steady state temperature and hydrogen blending. This further implies a complexity as to how geometric swirl number impacts the total heat transfer from a flame to a product. As previously shown, increasing S_g decreased radiative fraction.

The hypothesised relationship between radiative fraction and steady state steel slab temperature was not observed. This suggests that additional factors such as convective heat transfer contributed to the steady state temperature of the steel slab. Flame length and shape are expected to influence the total heat transfer from the flame, and the steady state temperature of the steel slab. Both flame length and shape are affected by S_g .

Changing the S_g of a burner will change a flame's length. By changing the flame length, the radiative heat flux profile will change. It has been previously shown that the location of maximum radiative heat flux is typically located at ~50–70 % along the flame's visible flame length. Since the steel slab was fixed for all cases, this location of maximum radiative heat flux will change, relative to the steel slab. Changing the S_g of a burner will also change the flame's shape. This will affect the temperature profile of the flame, relative to the steel slab. This change is expected to have a direct impact on the heat transfer to the steel slab. This infers how variations in burner characteristics, such as S_g , alter the effect of fuel switching on heating performance for a fixed product set-up.

Demonstrating this point further is the $S_g = 1.47$ case with 100 % hydrogen, which achieves the second-highest steady state steel slab temperature across all cases, 125 °C, despite registering the lowest radiative fraction, of all of the cases tested. When solely considering the radiative heat flux at a distance of 240 mm along the Z-axis, which corresponds to the height of the steel slab centreline, a direct correlation is still not apparent. The combination of a higher geometric swirl

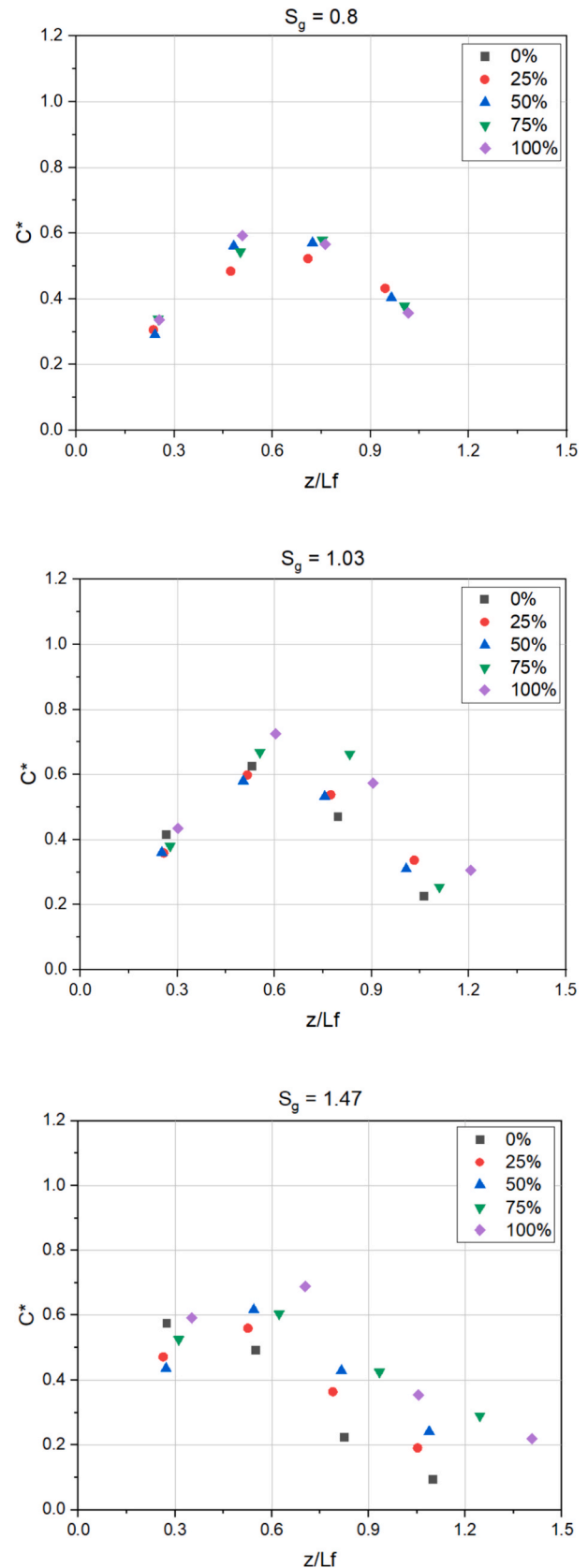


Fig. 11. Dimensionless radiative power C^* along the nominal length of the flame with respect to hydrogen blending and geometric swirl number.

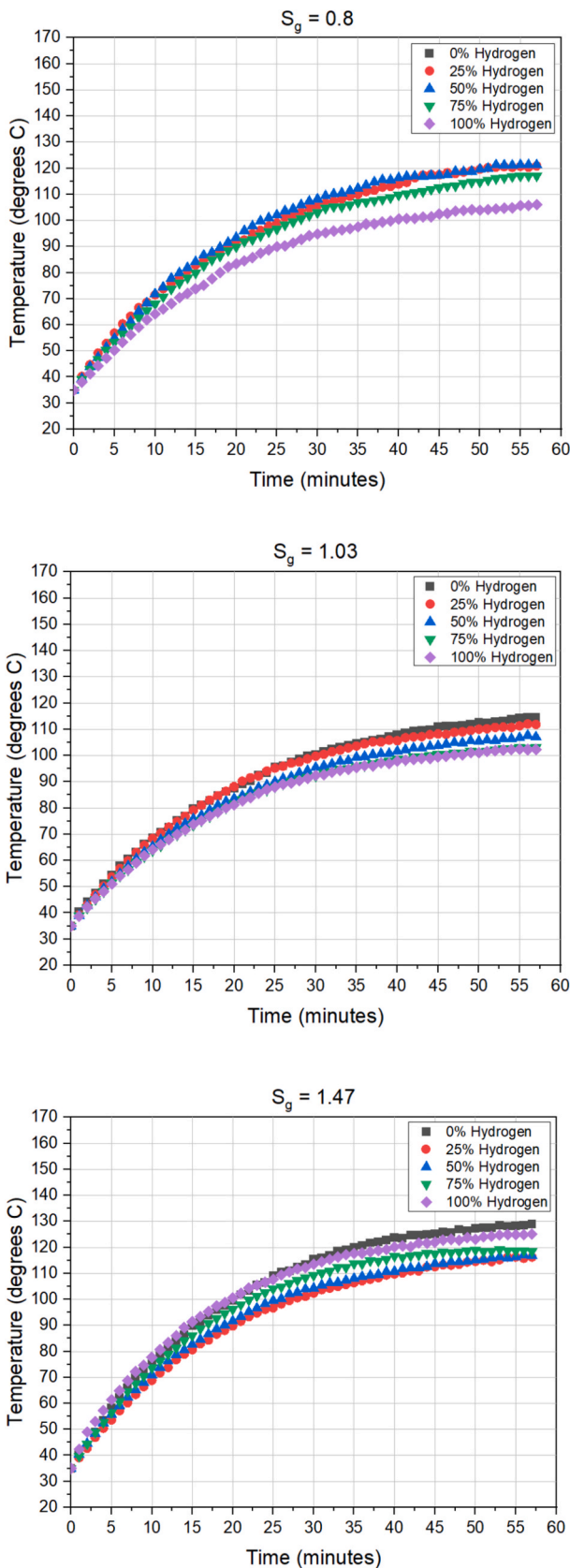


Fig. 12. The transient temperature response of the steel slab, 100 mm from the burner Z-axis centreline.

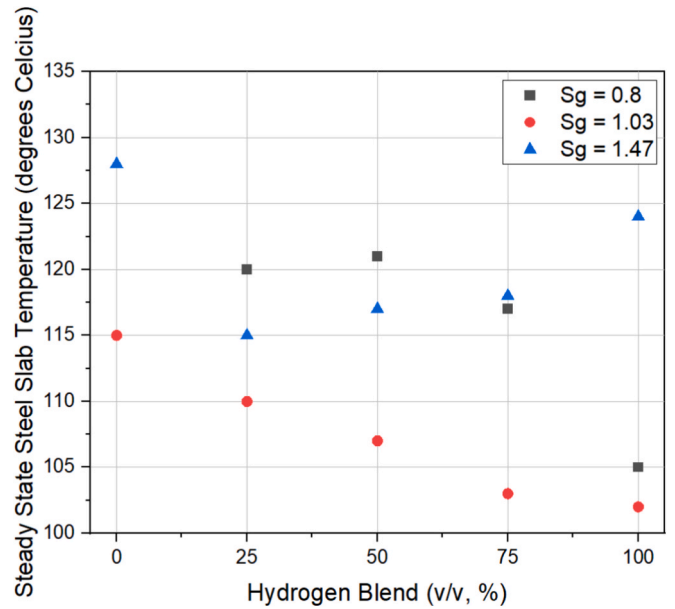


Fig. 13. Steady state slab temperatures with respect to hydrogen blending and geometric swirl number.

number, inducing a rise in flow turbulence, combined with a higher flame temperature at 240 mm of 1035 °C, necessitates consideration of convective heat transfer. It is suggested that notable convective heat transfer is actively occurring in this case, given the 100 mm proximity of the steel slab to the flame. Convective heat transfer depends on the proximity of the flow of hot combustion products heating the steel slab [41]. A distance of 100 mm enables the flow of hot combustion products directly contact the steel slab, paired with the shorter and wider flame shape associated with the $S_g = 1.47$.

The height at which the steel slab is located, relative to the flame, will influence the relative intensities of both radiative and convective heat transfer to the slab. Altering the location of this slab would introduce changes in the steady state steel slab temperature, and thus the relationships shown in Fig. 13. Changing the distance between the steel slab and the Z-axis centreline is also expected to have an impact on the magnitude of radiative and convective heat flux. For example, a flame with its maximum heat flux at 240 mm might yield steel slab temperatures that surpass those of a flame with higher heating properties, where the maximum point of heat transfer is not aligned with 240 mm. The heating performance of flames depends on the location of maximum radiative and convective heat flux, relative to the targeted product, intended for heating, making these results set-up specific. These results indicate that there are inherent differences between the practical heat transfer characteristics of hydrogen and methane flames.

In the work prior mentioned by Daurer et al. [17], the results are setup-dependent, with factors such as thermal input power and the fuel blend influencing the flame’s length and heat flux profile in a semi-industrial furnace, ultimately affecting how the product is heated and thus affecting the process efficiency. However, in that work, hydrogen blending resulted in an increase in process heating efficiency, that is not represented by Fig. 13, where no noticeable trend is present across the three geometric swirl burners that were tested. This does however align with the suggestion by Leicher et al. [13] that integrating hydrogen admixtures into industrial heating processes presents significant complexities amongst different processes. The integration requires a high degree of specialization and optimization to prevent any negative impact on process performance, given the unique characteristics of individual industrial heating systems.

For each geometric swirl number tested, the range in steel slab temperature in Fig. 13 is ~5–15 degrees Celsius. Although this may be

considered a small variation, this contradicts previous studies, which state no significant effect on product temperature with blends of up to 50 % hydrogen [11,12,14]. These differences may be explained by fundamental variations in experimental conditions. In this study, experiments were conducted without air preheating and at a lab scale, while the literature findings referenced here were obtained at a semi-industrial scale with air preheating ranging from 1150 to 1400 degrees Celsius. Additionally, the larger scale and whole-system approach in those studies may have influenced the results through factors such as direct flame impingement.

The findings of Xu et al. [16], in a lab-scale furnace without air preheating, show that when the flame is closely confined, with a lower confinement ratio than presented in this study, hydrogen flames result in a 15 % increase in heat transfer efficiency from the gas to the wall, compared to methane flames. In contrast, this study observed an unconfined flame, using a Gardon Gauge heat flux sensor, to directly measure radiative and convective heat transfer from the flame. This method sought to minimize the complex interactions between the wall, the flame, and the gas, providing a clearer understanding of the flame's behaviour. In this work, there is also an absence of reflective furnace walls due to the nature of the unconfined experimental set up. There remains the need for semi-industrial scale testing for up to 100 % hydrogen blending, assessing a broad range of industrial heating processes and experimental conditions, addressing the impact of reflective furnace walls and greater furnace temperatures.

To compare the differences in the 2-dimensional convective and radiative heat flux, pure hydrogen and methane flames were used. These measurements were taken along the flame's length, at 100 mm, 125 mm, and 150 mm radially from the burner Z-axis centreline. Measurements were taken by a Gardon Gauge, with and without a sapphire lens to distinguish the independent heat transfer modes. As shown in Fig. 14, the convective heat transfer exceeded that of radiative heat transfer. As previously mentioned, due to the relatively low local gas temperatures, when compared to large-scale industrial heating process, convection was expected to be the most dominant mode of heat transfer. If local gas temperatures were to exceed 1000 degrees Celsius, radiation would be expected to exceed convective heat transfer by an order of magnitude, accounting for ~90 % of the total heat transfer in an industrial furnace [8].

This study specifically measures radiation and convection directly from the reacting flame and its immediate exhaust gases, rather than including the heat transfer from large amounts of recirculating exhaust gases, that may be present in larger scale industrial heating processes. This data may not directly apply to large industrial furnaces in which this is the case. The process-dependent nature of heat transfer necessitates the scaling of this study for more specific industrial conditions. This experimental method serves as a crucial first step in understanding the overall mechanisms for heat transfer in high-temperature industrial processes.

Fig. 15 illustrates the ratio of local radiative heat flux to local convective heat flux, at various axial and radial positions. These measurements are plotted along the nominal axial position along the flame, z/L_f . The general trend shows that the radiation-to-convection ratio was highest near the burner nozzle and decreased with increasing axial distance along the flame's length. Beyond a flame's visible length, where $z/L_f > 1.0$, the majority of total heat flux is attributed to convective heat transfer. A noticeable deviation from this trend occurred close to the burner nozzle at $z/L_f \approx 0.3$, where methane flames exhibited notably higher radiation-to-convection ratios compared to hydrogen flames at the radial locations tested. This is likely due to the higher radiative heat flux of methane that was measured at this axial distance along the flame, as shown in Fig. 14.

In Fig. 16, a graph showing the relationship between local gas temperature measurements and local convective heat flux measurements is shown. This data was taken from a variety of axial and radial locations for both pure hydrogen and pure methane flames. As one might expect,

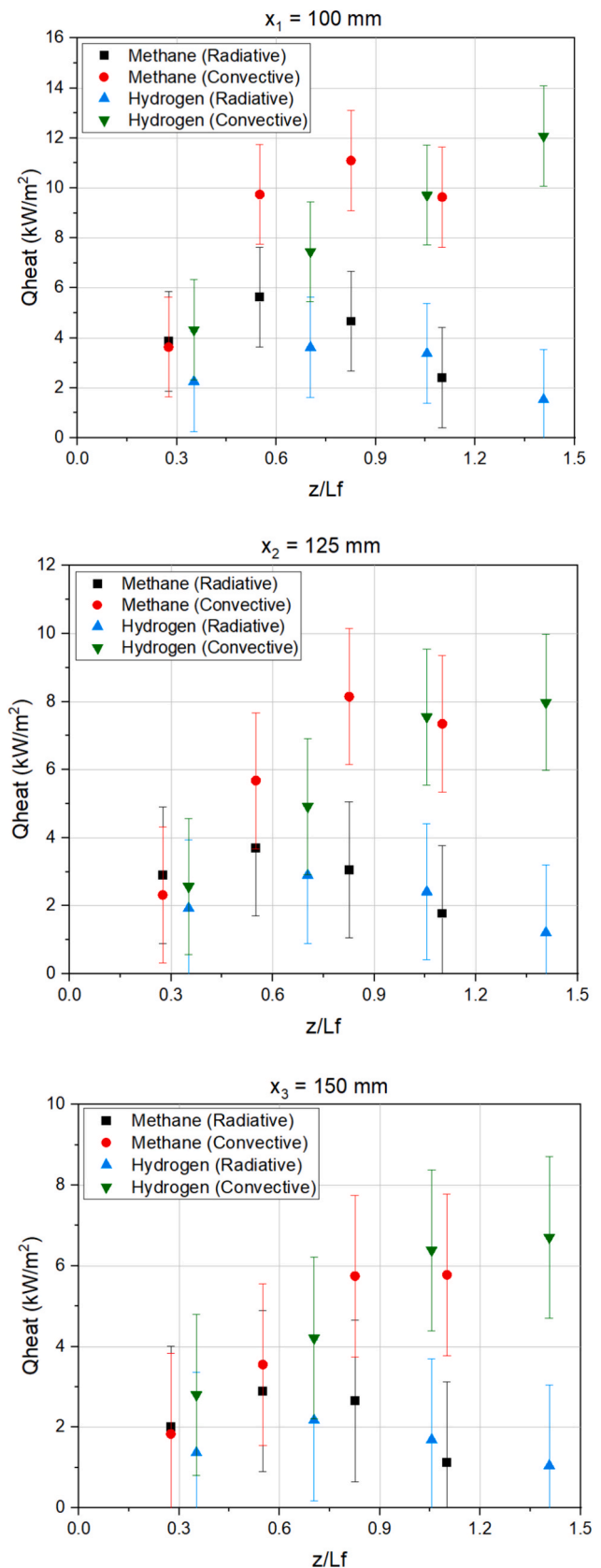


Fig. 14. The measured radiative and convective heat flux for both pure methane and pure hydrogen along the nominal length of the flame ($S_g = 1.47$).

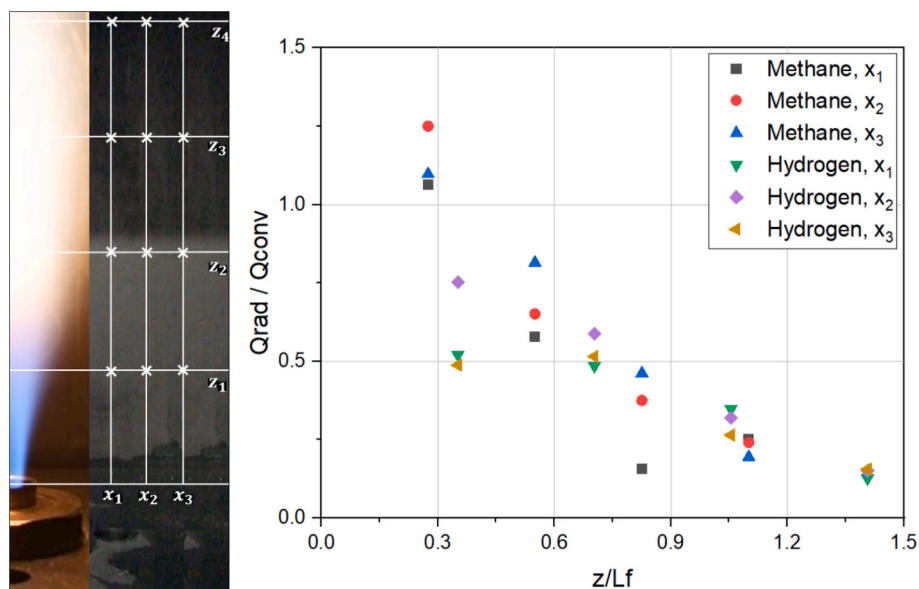


Fig. 15. The ratio of radiative to convective heat transfer modes of hydrogen and methane flames for a diffusion flame with $S_g = 1.47$ at 3 radial locations: x_1 , x_2 , x_3 .

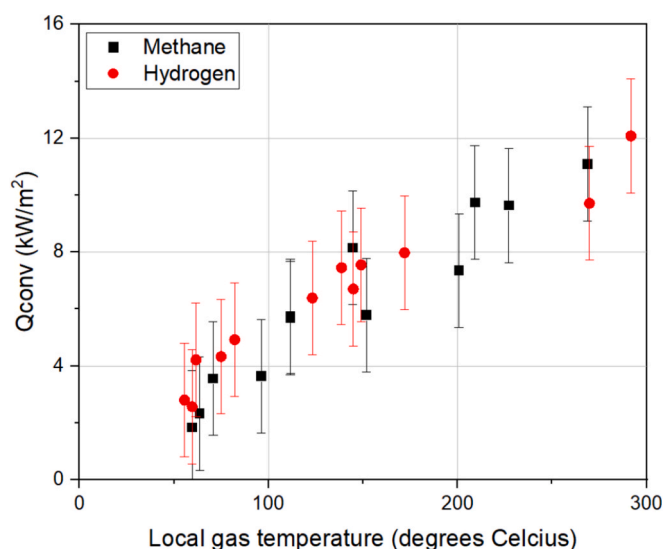


Fig. 16. The convective heat flux at a given location vs the measured local gas temperature at that given location ($S_g = 1.47$).

with increasing local gas temperature, the measured convective heat flux also increased. There is no pronounced impact of fuel type on this relationship. Much of this could be as a result of hot air being the convectively acting fluid at a distance of 100–150 mm from the burner centreline. This relationship is useful for industrial heating processes undergoing fuel switching, in that for the same temperature, a similar convective heat transfer can be expected across hydrogen and methane flames. This work did not consider direct flame impingement; this must be considered for industrial processes where there is direct contact between the flame and the heated product.

Hydrogen flames displayed greater flame temperatures closer to the burner nozzle. This was expected due to a hydrogen flame's faster rate of reaction [42] with shorter flame lengths, achieving maximum temperature earlier along the burner's Z-axis centreline than methane flames. Hydrogen also has a greater adiabatic flame temperature than methane, as previously shown in Table 1, predicting a greater maximum achievable temperature. Beyond the visible flame length, the measured

temperatures at the burner centreline decrease due to the shorter hydrogen flame length which is more pronounced at the locations tested than in methane flames.

It can be seen in Fig. 17, at the axial distances of 120 mm and 240 mm, that local gas temperatures are greater adjacent to methane flames than adjacent to hydrogen flames. This is suggested to be as a result of the higher radiative heat transfer from methane flames, transferring energy to the local air. Despite lower flame temperatures, methane flames produced higher radiative heat transfer, which is believed to be due to highly radiative species, such as soot and carbon dioxide, enhancing the emissivity of the flame. In turn, the elevated local gas temperatures enhance the local convective heat transfer at that location. Later in the flame, adjacent local gas temperatures continue to increase for both fuels. This is expected due to the expansion of the hot exhaust gases, facilitated further by the radial momentum of the swirling flow [23], in addition to the radiative heat transfer from the flame. The fluid dynamics of the flow field must be considered to further evaluate, not only the temperature profile of the flame, but also the convective heat flux profile of the flame.

4. Conclusion

Three geometric swirl numbers and five hydrogen-methane blends were studied to investigate their impact on heat transfer from flames. This work is a crucial first step in de-risking the path to net-zero for industrial heating processes. Key conclusions include:

- Higher hydrogen blending raised the adiabatic flame temperature, supported by experimental flame temperature measurements.
- A higher geometric swirl number reduced radiative fraction and visible flame lengths.
- For $S_g = 0.8$, radiative fraction decreased with increasing hydrogen blend, starting at 25 %.
- For $S_g = 1.03$, maximum radiative fraction was measured at 25 % hydrogen.
- For $S_g = 1.47$, maximum radiative fraction was measured at 50 % hydrogen, across all blends.
- Maximum radiative heat flux occurred at ~50–70 % along the visible flame length, as previously observed by Sivathanu et al [25].

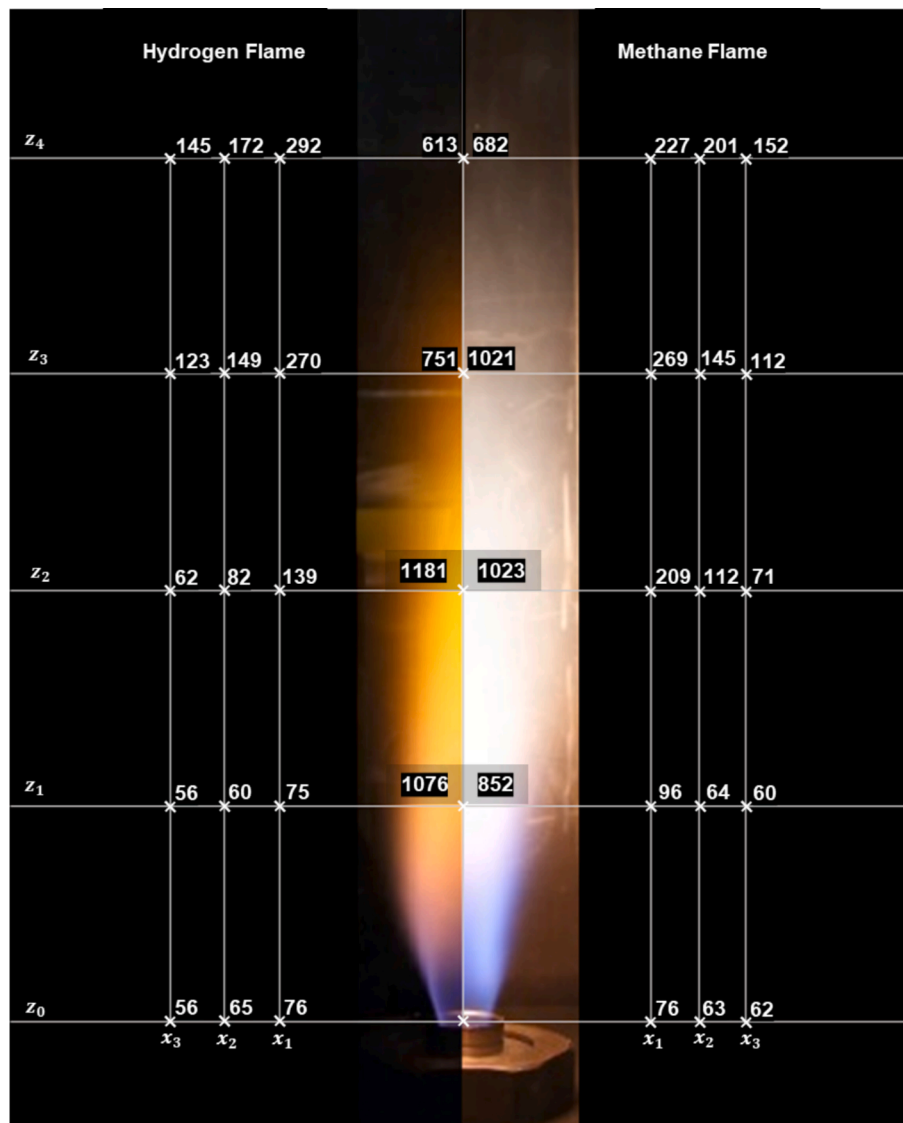


Fig. 17. Local temperature (Celsius) distribution of a hydrogen and methane flame ($S_g = 1.47$).

- As S_g increased, the distribution of nominal radiative power, C^* along the nominal flame length, z/L_f , deviated from the trend observed by Sivathanu et al [25].
- Local gas temperature correlated with convective heat flux, regardless of fuel choice.
- Radiation and convection intensity from the flame decreased similarly with increasing radial distance.
- The radiation-to-convection ratio from the flame was greatest near the burner nozzle and decreased with axial distance.

The steady-state temperatures of the steel slab are specific to this experimental setup. In larger, higher-temperature processes, radiative heat transfer is expected to have a more significant impact on overall heat transfer. In lower temperature processes with mostly convective heat transfer, local gas temperature measurements can assist in estimating changes in convective heat transfer, due to the strong correlation between the two, regardless of the fuel used.

To further de-risk industrial heating applications transitioning to hydrogen, these experiments should be scaled to model the specific process, accounting for relevant operational factors. Since this work has shown that the effect of fuel switching is process-dependent, this approach provides a more accurate representation of the process,

increasing confidence in the data obtained.

CRediT authorship contribution statement

Ben White: Writing – review & editing, Methodology, Investigation, Validation, Formal Analysis, Data Curation, Conceptualization. **Burak Goktepe:** Writing – review & editing, Validation, Data curation, Conceptualization. **Richard Marsh:** Writing – review & editing, Supervision, Funding acquisition, Conceptualization, Validation. **Steve Morris:** Writing – review & editing, Supervision, Methodology, Investigation. **Andrew Price:** Supervision, Conceptualization.

Declaration of competing interest

The authors declare that they have no known competing financial interests or personal relationships that could have appeared to influence the work reported in this paper.

Acknowledgements

This work has been supported by the EPSRC Centre for Doctoral Training in Resilient Decarbonised Fuel Energy Systems (Grant number:

EP/S022996/1), UKRI funded Industrial Decarbonisation Research Centre (IDRIC) and CR Plus, with the invaluable technical support and hard work from GTRC technician Jack Thomas.

Data availability

Data will be made available on request.

References

- [1] Department for Energy Security and Net Zero, "Net Zero Strategy: Build Back Greener," Apr. 2022. Accessed: Feb. 24, 2025. [Online]. Available: <https://www.gov.uk/government/publications/net-zero-strategy>.
- [2] Department for Energy Security and Net Zero, "UK Hydrogen Strategy," Dec. 2024. Accessed: Feb. 24, 2025. [Online]. Available: <https://www.gov.uk/government/publications/uk-hydrogen-strategy>.
- [3] Department of Energy Security and Net Zero, "Hydrogen Production Business Model," 2022. Accessed: Feb. 25, 2025. [Online]. Available: <https://www.gov.uk/government/publications/hydrogen-production-business-model>.
- [4] Anthony Green and Danielle Stewart, "Project Union Launch Report 2022," Warwick, 2022. Accessed: Feb. 25, 2025. [Online]. Available: <https://www.nation.algas.com/sites/default/files/documents/Project%20Union%20Executive%20Summary%20A4%20folded-JF-V15.pdf>.
- [5] SWIC, "A Plan For Clean Growth," 2023. Accessed: Feb. 25, 2025. [Online]. Available: <https://www.swic.cymru/clusterplan-reports>.
- [6] Department for Energy Security and Net Zero, "Hydrogen Blending into GB Gas Distribution Networks," 2023. Accessed: Feb. 25, 2025. [Online]. Available: <https://assets.publishing.service.gov.uk/media/650057d81886eb00139771f8/hydrogen-blending-into-gb-gas-distribution-networks-consultation.pdf>.
- [7] G. Martins, O.S.H. Mendoza, M. Amjad, E.P. Bandarra Filho, Geometric optimization of radiative heat transfer on surfaces of corrugated furnaces, *Appl. Therm. Eng.*, 104 (2016) 344–357, <https://doi.org/10.1016/j.applthermaleng.2016.05.070>.
- [8] P. Mullinger, B. Jenkins, Industrial and process furnaces, Third. Susan Dennis (2023), <https://doi.org/10.1016/C2020-0-04546-9>.
- [9] S. Chander, A. Ray, Flame impingement heat transfer: A review, *Energy Convers Manag* 46 (18–19) (Nov. 2005) 2803–2837, <https://doi.org/10.1016/j.enconman.2005.01.011>.
- [10] J. Leicher, A. Giese, C. Wieland, Electrification or hydrogen? the challenge of decarbonizing industrial (high-temperature) process heat, *J. (Basel)* 7 (4) (Oct. 2024) 439–456, <https://doi.org/10.3390/j7040026>.
- [11] B. Islami, A. Giese, M. Biebl, T. Nowakowski, "Impact of natural gas-hydrogen blends and pure hydrogen on combustion in glass melting furnaces, as well as spatially-resolved green hydrogen production potential in the German state of North Rhine-Westphalia (NRW). In Proceedings of the 97th DGG Glass Technology Conference, Aachen, Germany," May 2024.
- [12] Görner, and J. Overath, "Investigations into the use of natural gas/hydrogen blends and hydrogen for decarbonization in the glass industry. In Proceedings of the 13th International Conference on Industrial Furnaces and Boilers (INFUB13)," Albufeira, Portugal, Apr. 2022.
- [13] J. Leicher, "hydrogen for Industrial Process Heating: Challenges and Opportunities, Hydrogen for Decarbonization", Paris, France, Oct. 2022.
- [14] N. Meynet, G.-A. Grandin, C. Gobin, F. Lefebvre, D. Honoré, Experimental characterization of hydrogen impact on the flame structure and NOx emissions inside a semi-industrial furnace, France, Rouen, Apr. 2023.
- [15] M. Mayrhofer, M. Koller, P. Seemann, R. Prieler, C. Hochenauer, Assessment of natural gas/hydrogen blends as an alternative fuel for industrial heat treatment furnaces, *Int. J. Hydrogen Energy* 46 (41) (Jun. 2021) 21672–21686, <https://doi.org/10.1016/j.ijhydene.2021.03.228>.
- [16] S. Xu, Z. Tian, Y. Chen, S. Liang, Y. Tu, H. Liu, Effect of hydrogen-blending ratio and wall temperature on establishment, NO formation, and heat transfer of hydrogen-enriched methane MILD combustion, *Fuel* 369 (Aug. 2024) 131787, <https://doi.org/10.1016/j.fuel.2024.131787>.
- [17] G. Daurer, S. Schwarz, M. Demuth, C. Gaber, C. Hochenauer, Experimental and numerical analysis of industrial-type low-swirl combustion of hydrogen enriched natural gas including OH* chemiluminescence imaging, *Int. J. Hydrogen Energy* 80 (Aug. 2024) 890–906, <https://doi.org/10.1016/j.ijhydene.2024.07.119>.
- [18] W. Houf, R. Schefer, Predicting radiative heat fluxes and flammability envelopes from unintended releases of hydrogen, *Int. J. Hydrogen Energy* 32 (1) (Jan. 2007) 136–151, <https://doi.org/10.1016/j.ijhydene.2006.04.009>.
- [19] R. Schefer, W. Houf, B. Bourne, J. Colton, Spatial and radiative properties of an open-flame hydrogen plume, *Int. J. Hydrogen Energy* 31 (10) (Aug. 2006) 1332–1340, <https://doi.org/10.1016/j.ijhydene.2005.11.020>.
- [20] J.H. Frank, R.S. Barlow, C. Lundquist, Radiation and nitric oxide formation in turbulent non-premixed jet flames, *Proc. Combust. Inst.* 28 (1) (Jan. 2000) 447–454, [https://doi.org/10.1016/S0082-0784\(00\)80242-8](https://doi.org/10.1016/S0082-0784(00)80242-8).
- [21] S.R. Turns, F.H. Myhr, Oxides of nitrogen emissions from turbulent jet flames: Part I—Fuel effects and flame radiation, *Combust Flame* 87 (3–4) (Dec. 1991) 319–335, [https://doi.org/10.1016/0010-2180\(91\)90116-S](https://doi.org/10.1016/0010-2180(91)90116-S).
- [22] G. Wang, T.F. Guiberti, S. Cardona, C.A. Jimenez, W.L. Roberts, Effects of residence time on the NOx emissions of premixed ammonia-methane-air swirling flames at elevated pressure, *Proc. Combust. Inst.* 39 (4) (2023) 4277–4288, <https://doi.org/10.1016/j.proci.2022.07.141>.
- [23] N. Syred, M. Abdulsada, A. Griffiths, T. O'Doherty, P. Bowen, The effect of hydrogen containing fuel blends upon flashback in swirl burners, *Appl. Energy* 89 (1) (Jan. 2012) 106–110, <https://doi.org/10.1016/j.apenergy.2011.01.057>.
- [24] A.A. Hosseini, M. Ghodrat, M. Moghiman, S.H. Pourhoseini, Numerical study of inlet air swirl intensity effect of a methane-air diffusion flame on its combustion characteristics, *Case Stud. Therm. Eng.* 18 (Apr. 2020) 100610, <https://doi.org/10.1016/j.csite.2020.100610>.
- [25] Y. Sivathanu, J. Gore, Total radiative heat loss in jet flames from single point radiative flux measurements, *Combust Flame* 94 (3) (Aug. 1993) 265–270, [https://doi.org/10.1016/0010-2180\(93\)90073-C](https://doi.org/10.1016/0010-2180(93)90073-C).
- [26] G.M. Faeth, Swirl flows, *Combust Flame* 63 (1–2) (Jan. 1986) 311, [https://doi.org/10.1016/0010-2180\(86\)90133-1](https://doi.org/10.1016/0010-2180(86)90133-1).
- [27] R.W. Bilger, The structure of diffusion flames, *Combust. Sci. Technol.* 13 (1–6) (Jul. 1976) 155–170, <https://doi.org/10.1080/00102207608946733>.
- [28] J. Runyon, R. Marsh, P. Bowen, D. Pugh, A. Giles, S. Morris, Lean methane flame stability in a premixed generic swirl burner: Isothermal flow and atmospheric combustion characterization, *Exp. Therm. Fluid Sci.* 92 (Apr. 2018) 125–140, <https://doi.org/10.1016/j.expthermflsci.2017.11.019>.
- [29] Y. Tong, M. Li, M. Thern, J. Klingmann, "An experimental study of effects of confinement ratio on swirl stabilized flame macrostructures," in volume 1: Boilers and heat recovery steam generator; combustion turbines; energy water sustainability; fuels, combustion and material handling; heat exchangers, condensers, cooling systems, and balance-of-plant, *Am. Soc. Mech. Eng.* (Jun. 2017), <https://doi.org/10.1115/POWER-ICOPE2017-3064>.
- [30] L. Ji, J. Wang, W. Zhang, R. Mao, G. Hu, Z. Huang, Effect of confinement ratio on flame structure and blow-off characteristics of swirl flames, *Exp. Therm. Fluid Sci.* 135 (Jul. 2022) 110630, <https://doi.org/10.1016/j.expthermflsci.2022.110630>.
- [31] P.R.N. Childs, J.R. Greenwood, C.A. Long, "heat Tux Measurement Techniques," (1999).
- [32] Eric Hoeksema, "User Manual GG01: Gardon gauge water-cooled high heat flux sensor," Dec. 2024.
- [33] I.H. Malitson, M.J. Dodge, Refractive index and birefringence of synthetic sapphire, *J. Opt. Soc. Am* (1972) 1405.
- [34] E. R. Dobrovinskaya, L. A. Lytvynov, and V. Pishchik, "Properties of Sapphire," in *Sapphire*, Boston, MA: Springer US, 2009, pp. 55–176. doi: 10.1007/978-0-387-85695-7_2.
- [35] H. Sadiq, M.B. Wong, J. Tashan, R. Al-Mahaidi, X.-L. Zhao, Determination of steel emissivity for the temperature prediction of structural steel members in fire, *J. Mater. Civ. Eng.* 25 (2) (Feb. 2013) 167–173, [https://doi.org/10.1061/\(ASCE\)MT.1943-5533.0000607](https://doi.org/10.1061/(ASCE)MT.1943-5533.0000607).
- [36] T. Bello-Ochende, Suppression of natural convection and radiation heat losses in solar cavity receivers: A novel approach, *J. Phys. Conf. Ser.* 1378 (4) (Dec. 2019) 042050, <https://doi.org/10.1088/1742-6596/1378/4/042050>.
- [37] S. Jiménez, Relevance of heat conduction in the correction and interpretation of high temperature, fine wire thermocouple measurements, *Combust Flame* 240 (Jun. 2022) 112022, <https://doi.org/10.1016/j.combustflame.2022.112022>.
- [38] TC Direct, "How accurate is a thermocouple?," <https://www.tcdirect.co.uk/thermocouple-sensors/thermocouple-accuracies.aspx>.
- [39] Omega, "Thermocouple Types," <https://www.omega.com/en-us/resources/thermocouple-types>.
- [40] T. Okawa et al., "Fundamentals for power engineering," in *Fundamentals of Thermal and Nuclear Power Generation*, Elsevier, 2021, pp. 77–226. doi: 10.1016/B978-0-12-820733-8.00003-0.
- [41] B. Zhao, Derivation of unifying formulae for convective heat transfer in compressible flow fields, *Sci Rep* 11 (1) (Aug. 2021) 16762, <https://doi.org/10.1038/s41598-021-95810-0>.
- [42] M. Ilbas, A. Crayford, I. Yilmaz, P. Bowen, N. Syred, Laminar-burning velocities of hydrogen-air and hydrogen-methane-air mixtures: An experimental study, *Int. J. Hydrogen Energy* 31 (12) (Sep. 2006) 1768–1779, <https://doi.org/10.1016/j.ijhydene.2005.12.007>.